INTERNATIONAL JOURNAL FOR NUMERICAL METHODS IN FLUIDS
Int. J. Numer. Meth. Fluids 2007; **55**:431–454
Published online 14 March 2007 in Wiley InterScience (www.interscience.wiley.com). DOI: 10.1002/fld.1462

Solution of the 2-D shallow water equations with source terms in surface elevation splitting form

Dong-Jun Ma*, †, De-Jun Sun and Xie-Yuan Yin

School of Engineering Science, University of Science and Technology of China, Hefei 230027, China

SUMMARY

A vertex-centred finite-volume/finite-element method (FV/FEM) is developed for solving 2-D shallow water equations (SWEs) with source terms written in a surface elevation splitting form, which balances the flux gradients and source terms. The method is implemented on unstructured grids and the numerical scheme is based on a second-order MUSCL-like upwind Godunov FV discretization for inviscid fluxes and a classical Galerkin FE discretization for the viscous gradients and source terms. The main advantages are: (1) the discretization of SWE written in surface elevation splitting form satisfies the exact conservation property ($\mathscr{C}$-Property) naturally; (2) the simple centred-type discretization can be used for the source terms; (3) the method is suitable for both steady and unsteady shallow water problems; and (4) complex topography can be handled based on unstructured grids. The accuracy of the method was verified for both steady and unsteady problems, including discontinuous cases. The results indicate that the new method is accurate, simple, and robust. Copyright © 2007 John Wiley & Sons, Ltd.

Received 19 August 2004; Revised 17 January 2007; Accepted 19 January 2007

KEY WORDS: shallow water equations; source terms; unstructured; finite volume; MUSCL; upwind scheme

1. INTRODUCTION

In the past two decades, the numerical models based on the non-linear shallow water equations (SWEs) have attracted an upsurge of attention due to their wide applications in hydraulic, ocean and environmental engineering: dam breaks, hydraulic jump, bore wave propagation, open channel flows, tidal flows, etc. The generally applicable numerical approach should embody the following necessary features: simulating discontinuous flows accurately; handling both steady and transient flows; describing and incorporating complex topography; simulating both sub- and super-critical

*Correspondence to: Dong-Jun Ma, School of Engineering Science, University of Science and Technology of China, Hefei 230027, China.
†E-mail: mdj@ustc.edu.cn

conditions; considering the effect of irregular bed topography and shear stress; enabling various practical inflow/outflow conditions in the domain of interest.

An early major method is based on finite-difference discretization of SWEs using Cartesian grids [1]. The lack of alignment of coordinate lines with boundaries can lead to inaccuracies in the flow solution. An approach that overcomes this difficulty is the use of boundary-fitted grids [2, 3], where the governing equations need to be transformed from Cartesian to curvilinear coordinates. However, the system of equations is usually much more complicated in the transformed coordinates. The finite-element methods (FEMs) [4, 5] are more convenient for complex geometries, but they are relatively difficult to deal with discontinuities and the discretized non-linear algebraic equations have to be solved by the iteration process. Alternatively, finite-volume (FV) methods [6–9] with approximate Riemann solvers combine the simplicity of finite-difference methods with the geometric flexibility of FEMs. These methods can obtain accurate numerical results and capture discontinuities properly such as hydraulic jumps and bore waves. However, there remains the need to generate a suitable boundary-conforming mesh for complex geometries. A preferable way is to adopt an irregular, unstructured grid system. Recent work in this area has yielded some rather impressive results using cell-centred FV methods [10–13] and vertex-centred FV methods [14].

However, additional problems appear in solving SWEs with source terms relevant to bed topography and bed shear stress. For example, Ambrosi [15] observed that a problem occurred when simulating still water above an uneven bed. The usual centred discretization of the source terms leads to non-conservative scheme because of the imbalance between the flux gradients and source terms. Bermúdez and Vázquez [16, 17] proposed upwind methods for the treatment of the bed slope source terms. Hubbard and Garcia-Navarro [18] extended this numerical treatment to higher-order TVD schemes. LeVeque [19] developed a high-resolution method to balance the source terms and flux gradients. These methods not only improved the accuracy of the numerical solution significantly, but also increased the complexity. Recently, Zhou *et al.* [20] indicated the main error is caused by inaccurate reconstruction of water depth, and they developed a simple surface gradient method (SGM) for treating source terms based on an accurate reconstruction of the conservative variables at cell interfaces.

In this paper, we utilize another conservative hyperbolic version of the non-linear SWEs written in a surface elevation splitting form (see, e.g. References [12, 21]), which properly balances the flux gradients and source terms. It is proved that a stationary solution in terms of an exact 'conservation' property ($\mathscr{C}$-Property [16]) can be obtained using a simple centred discretization of source terms. The equations are discretized using a vertex-centred FV/FEM which has been successfully used in solving compressible viscous flows [22, 23]. Unlike the FV method used before, the FV/FEM is based on more robust mathematical theory and easy to establish the error estimates [24, 25]. A second-order MUSCL-like upwind Godunov FV method is used for the discretization of the inviscid fluxes in the resulting numerical method, and a linear classical Galerkin FEM, which is equivalent to the simple central-type discretization in code implementation, is applied to the evaluation of viscous gradients and source terms. The construction of an approximate Jacobian (Roe type) of the normal flux function is proposed. The time integration scheme employs the second-order predictor–corrector method. The general inflow, outflow, wall and non-reflecting boundary conditions are also discussed according to the characteristic theory. Results are presented for a series of validation tests designed to verify the accuracy and applicability of the FV/FEM. The tests include simulations of 1-D stationary problem, unsteady moving fronts (i.e. dam break), flow recirculation (jet-forced flow in a reservoir), steady shock-type discontinuity (hydraulic jump), and a quasi-steady problem with small perturbation.

DOI: 10.1002/fld

2. GOVERNING EQUATIONS

Vertical integration of the 3-D incompressible Navier–Stokes equations along with the assumptions of a hydrostatic pressure and a vertically uniform horizontal velocity profile, results in the SWEs written as the following conservative differential form [26]:

$$\frac{\partial \zeta}{\partial t} + \frac{\partial (uh)}{\partial x} + \frac{\partial (vh)}{\partial y} = 0$$

$$\frac{\partial (uh)}{\partial t} + \frac{\partial (u^2 h)}{\partial x} + \frac{\partial (uvh)}{\partial y} - \nu \left(\frac{\partial (hu_x)}{\partial x} + \frac{\partial (hu_y)}{\partial y} \right) = \frac{\tau_{wx} - \tau_{bx}}{\rho} - gh \frac{\partial \zeta}{\partial x} + hf_c v \tag{1}$$

$$\frac{\partial (vh)}{\partial t} + \frac{\partial (uvh)}{\partial x} + \frac{\partial (v^2 h)}{\partial y} - \nu \left(\frac{\partial (hv_x)}{\partial x} + \frac{\partial (hv_y)}{\partial y} \right) = \frac{\tau_{wy} - \tau_{by}}{\rho} - gh \frac{\partial \zeta}{\partial y} - hf_c u$$

where ζ is the free water surface elevation above a fixed reference water level, $h = h_b + \zeta$ is the total water depth, and h_b is the partial depth between the fixed reference level and the bed surface (see Figure 1). u and v are depth-averaged velocity components in the horizontal x- and y-directions, respectively, u_x, u_y and v_x, v_y are derivatives of the depth-averaged velocity components. g is the acceleration due to gravity, ρ the water density, f_c the Coriolis parameter and ν the kinematic eddy viscosity coefficient. τ_{bx} and τ_{by} are the bed friction shear stresses in the x- and y-directions, respectively, τ_{wx} and τ_{wy} are the surface shear stresses.

Usually, the $\partial \zeta / \partial t$ is written as $\partial h / \partial t$, and the term $gh \partial \zeta / \partial x$ is split to give the hyperbolic formulation (e.g. [7, 10])

$$gh \frac{\partial \zeta}{\partial x} = \frac{1}{2} g \frac{\partial h^2}{\partial x} + ghS_{ox}, \quad S_{ox} = \frac{\partial z_b}{\partial x} = -\frac{\partial h_b}{\partial x} \tag{2}$$

where S_{ox} is the bed slope in the x-direction and z_b the bed surface height. However, the split of the free surface gradient term causes an imbalance between the source and flux gradient components, and the centred discretization of the source terms leads to non-conservative scheme [16]. A consequence of using the conventional methods is that even the still water cannot be

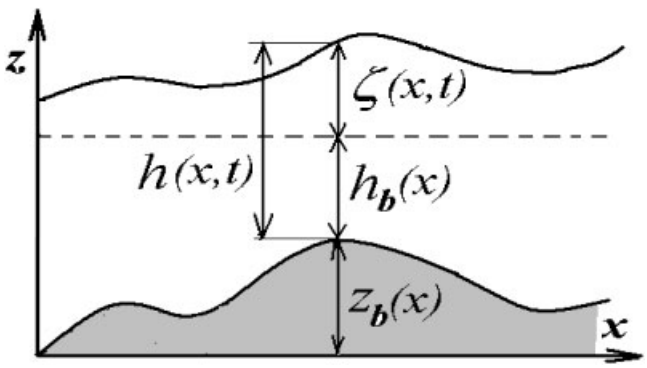

Figure 1. Definition for bed topography.

DOI: 10.1002/fld

calculated exactly. The difficulty can be overcome by upwind discretization of the source terms [16–18], which balance the flux gradients and source terms. The main drawback of this method is of its complexity. Another explanation for inaccuracies of the solution is the values of water depth reconstructed are not exact at the cell interface when the usual high-resolution Godunov-type methods are utilized with a centred discretization for the bed slope terms [20].

An alternative splitting and redistributing method for the term $gh\partial\zeta/\partial x$ described in [12, 21] is employed to overcome the above difficulty, which matches the idea of using water surface elevation reconstruction [20] to balance the flux gradients and source terms

$$gh\frac{\partial\zeta}{\partial x}=\frac{1}{2}g\frac{\partial(h^2-h_b^2)}{\partial x}+g\zeta S_{ox} \tag{3}$$

The resulting formulation still retains the hyperbolic nature of the SWE, so the sophisticated numerical methods for SWE in water depth form can be utilized only with a little modification, such as the Roe scheme. The water surface elevation reconstruction is decoupled from bed surface variation, which is always included in the water depth and should be considered carefully to balance the flux gradients and source terms as in SGM [20]. Because we use surface elevation to replace water depth in SWE, the centred-type discretization can be utilized for the bed slope source terms like SGM, but not the complex upwind discretization. The new formulations can be written as

$$\frac{\partial\zeta}{\partial t}+\frac{\partial(uh)}{\partial x}+\frac{\partial(vh)}{\partial y}=0$$

$$\begin{aligned}&\frac{\partial(uh)}{\partial t}+\frac{\partial(u^2h+\frac{1}{2}g(h^2-h_b^2))}{\partial x}+\frac{\partial(uvh)}{\partial y}-v\left(\frac{\partial(hu_x)}{\partial x}+\frac{\partial(hu_y)}{\partial y}\right)\\&=\frac{\tau_{wx}-\tau_{bx}}{\rho}-g\zeta S_{ox}+hf_{\mathrm{c}}v\end{aligned} \tag{4}$$

$$\begin{aligned}&\frac{\partial(vh)}{\partial t}+\frac{\partial(uvh)}{\partial x}+\frac{\partial(v^2h+\frac{1}{2}g(h^2-h_b^2))}{\partial y}-v\left(\frac{\partial(hv_x)}{\partial x}+\frac{\partial(hv_y)}{\partial y}\right)\\&=\frac{\tau_{wy}-\tau_{by}}{\rho}-g\zeta S_{oy}-hf_{\mathrm{c}}u\end{aligned}$$

where S_{oy} is the bed slope in the y-direction. The bed friction shear stresses are defined as

$$\tau_{bx}=\frac{\rho gu\sqrt{u^2+v^2}}{C_z^2}=\frac{\rho gn^2u\sqrt{u^2+v^2}}{h^{1/3}},\quad \tau_{by}=\frac{\rho gv\sqrt{u^2+v^2}}{C_z^2}=\frac{\rho gn^2v\sqrt{u^2+v^2}}{h^{1/3}} \tag{5}$$

where C_z is the Chezy friction coefficient and n the Mannings roughness coefficient.

And the SWE can be written in the vectorial form

$$\underbrace{\frac{\partial\mathbf{U}}{\partial t}}_{\text{temporal derivative}}+\underbrace{\nabla\cdot\mathbf{F}}_{\text{inviscid fluxes}}=\underbrace{v\nabla\cdot\mathbf{R}}_{\text{viscous terms}}+\underbrace{\mathbf{S}}_{\text{source terms}} \tag{6}$$

DOI: 10.1002/fld

where $\nabla = \mathbf{i}(\partial/\partial x) + \mathbf{j}(\partial/\partial y)$, $\mathbf{F} = \mathbf{F}^x\mathbf{i} + \mathbf{F}^y\mathbf{j}$, $\mathbf{R} = \mathbf{R}^x\mathbf{i} + \mathbf{R}^y\mathbf{j}$, and

$$\mathbf{U} = \begin{pmatrix} \zeta \\ uh \\ vh \end{pmatrix}, \quad \mathbf{F}^x = \begin{pmatrix} uh \\ u^2h + \frac{1}{2}g(h^2 - h_b^2) \\ uvh \end{pmatrix}, \quad \mathbf{F}^y = \begin{pmatrix} vh \\ uvh \\ v^2h + \frac{1}{2}g(h^2 - h_b^2) \end{pmatrix}$$

$$\mathbf{R}^x = \begin{pmatrix} 0 \\ h\,\partial u/\partial x \\ h\,\partial v/\partial x \end{pmatrix}, \quad \mathbf{R}^y = \begin{pmatrix} 0 \\ h\,\partial u/\partial y \\ h\,\partial v/\partial y \end{pmatrix}, \quad \mathbf{S} = \mathbf{S}_b + \mathbf{S}_p$$

$$\mathbf{S}_b = \begin{pmatrix} 0 \\ -g\zeta S_{ox} \\ -g\zeta S_{oy} \end{pmatrix}, \quad \mathbf{S}_p = \begin{pmatrix} 0 \\ (\tau_{wx} - \tau_{bx})/\rho + hf_c v \\ (\tau_{wy} - \tau_{by})/\rho - hf_c u \end{pmatrix}$$

We will consider the initial and boundary value problem (IBVP) (let $\Omega \subset \mathbb{R}^2$ be the flow domain and Γ be its boundary).

$$\begin{aligned} &\frac{\partial \mathbf{U}}{\partial t} + \nabla \cdot \mathbf{F}(\mathbf{U}, X) = \nu \nabla \cdot \mathbf{R}(\mathbf{U}) + \mathbf{S}(\mathbf{U}, X), \quad (X, t) \in \Omega \times \mathbb{R}^+ \\ &\mathbf{U}(X, 0) = \mathbf{U}_0(X), \quad X \in \Omega \\ &\mathbf{U}(X, t) = \mathbf{U}_\Gamma(X), \quad X \in \Gamma = \partial\Omega \\ &h_b(X, t) = h_{b0}(X), \quad X \in \Omega \end{aligned} \tag{7}$$

where $\mathbf{U}_0$, $\mathbf{U}_\Gamma$ and h_{b0} are specified functions, and focus on finding a weak solution of (7).

3. MIXED FINITE-VOLUME/FINITE-ELEMENT METHOD

The numerical method is a mixed FV/FEM using a second-order accurate monotonic upwind scheme for conservation laws (MUSCL) on fully unstructured grids for 2-D SWE. The spatial approximation combines an upwind FVM for the discretization of the non-linear inviscid terms with a classical Galerkin (piecewise linear) FEM for the discretization of the viscous and source terms, which is equivalent to a simple central-type discretization in code implementation.

3.1. Dual finite-volume mesh

The computational region Ω is assumed to be a polygonal bounded domain of $\mathbb{R}^2$. Let $\mathscr{T}_h$ be a standard FE triangulation of Ω, and $l_{\max}$ the maximal length of the edges in $\mathscr{T}_h$. A vertex of a triangle $\triangle$ is denoted by P_i, and the set of its neighbouring vertices by $N(i)$.

A dual FV mesh can be built such that there exists a bijective operator from the FE mesh to the FV mesh and the FV mesh covers exactly the domain Ω. As shown in Figure 2, at each vertex P_i, the control volume C_i is constructed as the union of the sub-triangles resulting from the

DOI: 10.1002/fld

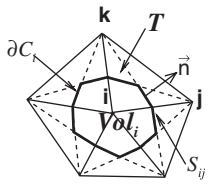

Figure 2. Control volume C_i in 2D.

subdivision by means of the medians of each triangle of $\mathscr{T}_h$ that is connected to P_i. The boundary of C_i is denoted by ∂C_i and the unit vector of the outward normal to ∂C_i by $\mathbf{n}_i = (n_{ix}, n_{iy})$. The union of all the constructed cells forms a non-overlapping partition of the domain Ω:

$$\Omega = \bigcup_{i=1}^{\text{ns}} C_i \tag{8}$$

Also, the following discrete spaces are introduced:

$$\begin{aligned} \mathscr{V}_h &= \{v_h | v_h \in C^0(\Omega),\ \ v_h|_{\triangle} \in P_1, \forall \triangle \in \mathscr{T}_h\} \\ \mathscr{W}_h &= \{v_h | v_h \in L^2(\Omega),\ \ v_h|_{C_i} = v_i = \text{constant},\ \ i = 1, \ldots, \text{ns}\} \end{aligned} \tag{9}$$

where P_1 is the polynomials space of order 1 and ns the total number of vertexes.

For each cell C_i a characteristic function φ_i is defined as

$$\varphi_i(X) = \begin{cases} 1 & \text{if } X \in C_i \\ 0 & \text{otherwise} \end{cases} \tag{10}$$

For any function f in $\mathscr{V}_h$, it can be determined by the vertex P_i value $f(P_i)$

$$f(X) = \sum_{i=1,\text{ns}} f(P_i)\phi_i(X) \tag{11}$$

where $\{\phi_i\}_{i=1}^{i=\text{ns}}$ is a basis of $\mathscr{V}_h$.

Finally, the natural bijection between the spaces $\mathscr{V}_h$ and $\mathscr{W}_h$ can be constructed as

$$B(f(X)) = \sum_{i=1,\text{ns}} f(P_i)\varphi_i(X) \quad \forall f \in \mathscr{V}_h \tag{12}$$

3.2. Weighted residual formulation

A weighted residual formulation of the IBVP is as follows: find $\mathbf{U} \in (\mathscr{V}_h)^3, \forall \psi_h \in \mathscr{V}_h$

$$\int_\Omega \frac{\partial \mathbf{U}}{\partial t}\psi_h \, \mathrm{d}\Omega + \int_\Omega (\nabla \cdot \mathbf{F} - \mathbf{S}_b)\psi_h \, \mathrm{d}\Omega = \int_\Omega (v\nabla \cdot \mathbf{R} + \mathbf{S}_p)\psi_h \, \mathrm{d}\Omega \tag{13}$$

A mixed FV/FE (Galerkin) approximation can be constructed by using the usual piecewise linear FE basis function ϕ_i as the test function for the viscous and source terms and applying the

DOI: 10.1002/fld

operator B to the left-hand side of (13) which lead to a mass-lumped weighted residual approach. And the above equation is transformed into

$$\int_{C_i} \frac{\partial \mathbf{U}}{\partial t}\,\mathrm{d}\Omega + \int_{C_i} (\nabla \cdot \mathbf{F} - \mathbf{S}_b)\,\mathrm{d}\Omega = \int_{\sum \triangle,\, P_i \in \triangle} (v\nabla \cdot \mathbf{R} + \mathbf{S}_p)\phi_i\,\mathrm{d}\Omega \tag{14}$$

Here $\sum \triangle,\ P_i \in \triangle$ means the sum of triangles, which include vertex P_i. Green's theorem is applied to the inviscid fluxes, while the viscous and source terms are integrated by parts, then

$$\int_{C_i} \frac{\partial \mathbf{U}}{\partial t}\,\mathrm{d}\Omega + \oint_{\partial C_i} \mathbf{F} \cdot \mathbf{n}\,\mathrm{d}\sigma = \int_{C_i} \mathbf{S}_b\,\mathrm{d}\Omega - \sum_{\triangle,\, P_i \in \triangle} \int_{\triangle} (v\mathbf{R} \cdot \nabla \phi_i^{\triangle} - \mathbf{S}_p \phi_i^{\triangle})\,\mathrm{d}\Omega + \oint_{\Gamma} \mathbf{R} \cdot \mathbf{n}\phi_i\,\mathrm{d}\sigma \tag{15}$$

and $\phi_i^{\triangle}$ is the restriction of ϕ_i to triangle $\triangle$. Finally, we drop the right-hand side boundary integral if we neglect the viscous stress effects on the boundary, so that (15) is simplified to

$$\begin{aligned} &\frac{\partial}{\partial t} \int_{C_i} \mathbf{U}\,\mathrm{d}\Omega + \sum_{j \in N(i)} \int_{\partial C_{ij}} \mathbf{F} \cdot \mathbf{n}_{ij}\,\mathrm{d}\sigma + \int_{\partial C_i \cap \Gamma} \mathbf{F} \cdot \mathbf{n}_i\,\mathrm{d}\sigma \\ &\quad = \int_{C_i} \mathbf{S}_b\,\mathrm{d}\Omega - \sum_{\triangle,\, P_i \in \triangle} \int_{\triangle} (v\mathbf{R} \cdot \nabla \phi_i^{\triangle} - \mathbf{S}_p \phi_i^{\triangle})\,\mathrm{d}\Omega \end{aligned} \tag{16}$$

3.3. Inviscid fluxes discretization

The inviscid fluxes can be evaluated by adopting upwind numerical fluxes at each cell edge. The numerical flux function $\mathbf{\Phi}$ of a first-order-accurate upwind scheme can be written as

$$\sum_{j \in N(i)} \int_{\partial C_{ij}} \mathbf{F} \cdot \mathbf{n}_{ij}\,\mathrm{d}\sigma = \sum_{j \in N(i)} \mathbf{\Phi}(\mathbf{U}_i, \mathbf{U}_j, \mathbf{n}_{ij}) \tag{17}$$

where

$$\mathbf{F} \cdot \mathbf{n} = \begin{pmatrix} h(un_x + vn_y) \\ uh(un_x + vn_y) + g(h^2 - h_b^2)n_x/2 \\ vh(un_x + vn_y) + g(h^2 - h_b^2)n_y/2 \end{pmatrix}$$

The flux difference splitting or flux vector splitting techniques can be adopted here. In our implementation, the upwind flux is obtained by solving a local Riemann problem in the direction normal to the cell interface. The numerical flux function used in the Roe approximate Riemann solver has the following form:

$$\mathbf{\Phi}(\mathbf{U}_{ij}^{\mathrm{R}}, \mathbf{U}_{ij}^{\mathrm{L}}, \mathbf{n}_{ij}) = \tfrac{1}{2}[\mathbf{F}(\mathbf{U}_{ij}^{\mathrm{R}}) + \mathbf{F}(\mathbf{U}_{ij}^{\mathrm{L}}) - |\mathbf{A}|(\mathbf{U}_{ij}^{\mathrm{R}} - \mathbf{U}_{ij}^{\mathrm{L}})] \cdot \mathbf{n}_{ij} \tag{18}$$

in which

$$|\mathbf{A}| = \mathbf{R}|\mathbf{\Lambda}|\mathbf{L}$$

where $\mathbf{U}_{ij}^{\mathrm{R}}$ and $\mathbf{U}_{ij}^{\mathrm{L}}$ are the reconstructed right and left Riemann states, respectively, at the cell interface ∂C_{ij} between adjacent cell i and j. $\mathbf{A}$ is the flux Jacobian matrix evaluated using $\mathbf{R}$ and

DOI: 10.1002/fld

L, the right and left eigenvector matrix of **A**, respectively (see [12, 27] in detail). And **Λ** is the diagonal matrix of the eigenvalues of **A**. The Jacobian matrix **A** is given by

$$\mathbf{A}=\frac{\partial(\mathbf{F}\cdot\mathbf{n})}{\partial\mathbf{U}}=\begin{pmatrix}0 & n_x & n_y\\ (c^2-u^2)n_x-uvn_y & 2un_x+vn_y & un_y\\ -uvn_x+(c^2-v^2)n_y & vn_x & un_x+2vn_y\end{pmatrix} \tag{19}$$

Following the technique used by Roe, we have searched for a modified matrix with eigenvalues of the form

$$\tilde{\lambda}_1=\tilde{u}n_x+\tilde{v}n_y+\tilde{c},\quad \tilde{\lambda}_2=\tilde{u}n_x+\tilde{v}n_y,\quad \tilde{\lambda}_3=\tilde{u}n_x+\tilde{v}n_y-\tilde{c} \tag{20}$$

and eigenvectors of the form

$$\tilde{\mathbf{e}}_1=\begin{pmatrix}1\\ \tilde{u}+\tilde{c}n_x\\ \tilde{v}+\tilde{c}n_y\end{pmatrix},\quad \tilde{\mathbf{e}}_2=\begin{pmatrix}0\\ -\tilde{c}n_y\\ \tilde{c}n_x\end{pmatrix},\quad \tilde{\mathbf{e}}_3=\begin{pmatrix}1\\ \tilde{u}-\tilde{c}n_x\\ \tilde{v}-\tilde{c}n_y\end{pmatrix} \tag{21}$$

The Roe average states $\tilde{u}$, $\tilde{v}$ and $\tilde{c}$ are given by

$$\tilde{u}=\frac{u^{\mathrm{L}}\sqrt{h^{\mathrm{L}}}+u^{\mathrm{R}}\sqrt{h^{\mathrm{R}}}}{\sqrt{h^{\mathrm{L}}}+\sqrt{h^{\mathrm{R}}}},\quad \tilde{v}=\frac{v^{\mathrm{L}}\sqrt{h^{\mathrm{L}}}+v^{\mathrm{R}}\sqrt{h^{\mathrm{R}}}}{\sqrt{h^{\mathrm{L}}}+\sqrt{h^{\mathrm{R}}}},\quad \tilde{c}=\sqrt{\frac{g(h^{\mathrm{L}}+h^{\mathrm{R}})}{2}} \tag{22}$$

Using the approximate Jacobian matrix $\tilde{\mathbf{A}}$, the numerical flux can be transformed as

$$\mathbf{\Phi}=\frac{1}{2}\left[\mathbf{F}^{\mathrm{L}}+\sum_{k=1}^{3}\tilde{\alpha}_k\min(0,\tilde{\lambda}_k)\tilde{\mathbf{e}}_k\right]\cdot\mathbf{n}_{ij}=\frac{1}{2}\left[\mathbf{F}^{\mathrm{R}}+\mathbf{F}^{\mathrm{L}}-\sum_{k=1}^{3}\tilde{\alpha}_k|\tilde{\lambda}_k|\tilde{\mathbf{e}}_k\right]\cdot\mathbf{n}_{ij} \tag{23}$$

where $\tilde{\alpha}_k(k=1,2,3)$ are the wave strengths as well as the coefficients of the decomposition in the basis of eigenvectors of $\tilde{\mathbf{A}}$

$$\mathbf{U}^{\mathrm{R}}-\mathbf{U}^{\mathrm{L}}=\sum_{k=1}^{3}\tilde{\alpha}_k\tilde{\mathbf{e}}_k \tag{24}$$

and are dependent on the jumps $\triangle=(\,)^{\mathrm{R}}-(\,)^{\mathrm{L}}$ in the functions:

$$\tilde{\alpha}_{1,3}=\frac{\triangle\zeta}{2}\pm\frac{1}{2\tilde{c}}[\triangle(hu)n_x+\triangle(hv)n_y-(\tilde{u}n_x+\tilde{v}n_y)\triangle\zeta] \tag{25a}$$

$$\tilde{\alpha}_2=\frac{1}{\tilde{c}}\{[\triangle(hv)-\tilde{v}\triangle\zeta]n_x-[\triangle(hu)-\tilde{u}\triangle\zeta]n_y\} \tag{25b}$$

3.4. High-order extension and limiters

The numerical integration with an upwind scheme described above leads to an approximation which is only first-order accurate in space. A second-order van Leer's MUSCL method extension [28] is

DOI: 10.1002/fld

utilized where the piecewise constant approximation is replaced by piecewise linear approximation to reconstruct the state at the cell interface, i.e. $\mathbf{U}^{\mathrm{L}}$ and $\mathbf{U}^{\mathrm{R}}$ between node i and j

$$\mathbf{U}^{\mathrm{L}} = \mathbf{U}_i + \tfrac{1}{2}\nabla\mathbf{U}_i \cdot \mathbf{n}_{ij}, \quad \mathbf{U}^{\mathrm{R}} = \mathbf{U}_j - \tfrac{1}{2}\nabla\mathbf{U}_j \cdot \mathbf{n}_{ij} \tag{26}$$

A second-order approximation requires the evaluation of the gradient of the conservative variables at each vertex. Clearly, the gradient of a function v_h of $\mathscr{V}_h$ is constant in each element and discontinuous in the flow domain. Using a linear interpolation of the Galerkin gradients computed in each triangle of C_i, the gradients $\nabla\mathbf{U}_i$ can be given as

$$\nabla\mathbf{U}_i = \frac{\int_{C_i} \nabla\mathbf{U}\,\mathrm{d}\Omega}{\int_{C_i} \mathrm{d}\Omega} = \frac{1}{\mathrm{area}(C_i)} \sum_{\triangle, P_i \in \triangle} \frac{\mathrm{area}(\triangle)}{3} \sum_{k \in \triangle} \mathbf{U}_k \nabla \phi_k^{\triangle} \tag{27}$$

where $k \in \triangle$ means the loop of three vertexes on triangle $\triangle$.

However, numerical oscillations may occur and are highly desirable to be eliminated when trying to simulate flow discontinuities. The main techniques used to control or limit spurious oscillations around discontinuities are to utilize artificial viscosity or make use of non-linear limiters. Slope limiters suppress the numerical oscillations in a non-linear manner by prohibiting the generation of any new local extrema when the conservative variables ζ, uh, vh are reconstructed at the cell interface.

In order to maintain monotonicity, the non-linear limiters restrict the variables gradients discussed previously, so that the cell interface state, i.e. $\mathbf{U}^{\mathrm{L}}$ or $\mathbf{U}^{\mathrm{R}}$ falls within the vertex variables in either side of the cell interface. As a result, the second-order cell interface variables reconstruction is limited in the following form:

$$\begin{aligned} \mathbf{U}^{\mathrm{L}} &= \mathbf{U}_i + 0.5\,\mathrm{Lim}((\nabla\mathbf{U})_i^{\mathrm{upwind}} \cdot \mathbf{n}_{ij}, (\nabla\mathbf{U})_i^{\mathrm{cent}} \cdot \mathbf{n}_{ij}) \\ \mathbf{U}^{\mathrm{R}} &= \mathbf{U}_j - 0.5\,\mathrm{Lim}((\nabla\mathbf{U})_j^{\mathrm{upwind}} \cdot \mathbf{n}_{ij}, (\nabla\mathbf{U})_j^{\mathrm{cent}} \cdot \mathbf{n}_{ij}) \end{aligned} \tag{28}$$

where

$$(\nabla\mathbf{U})_i^{\mathrm{cent}} \cdot \mathbf{n}_{ij} = \mathbf{U}_j - \mathbf{U}_i$$

$$(\nabla\mathbf{U})_i^{\mathrm{upwind}} = 2\nabla\mathbf{U}_i - (\nabla\mathbf{U})_i^{\mathrm{cent}}$$

and the non-linear limiter

$$\mathrm{Lim}(a, b) = b \max\left[0, \min\left(\beta\frac{a}{b}, 1\right), \min\left(\frac{a}{b}, \beta\right)\right] \tag{29}$$

where the limiter parameter, β, is restricted to $1 \leqslant \beta \leqslant 2$. In particular, $\beta = 1$ gives the minmod limiter, and $\beta = 2$ gives the Roe Superbee limiter. Usually the super-bee limiter is less diffusive and gives an excessively steep profile with some oscillation, while the minmod limiter produces a relatively smeared profile and so is slightly dissipative. As the limiter increases in strength, it is less diffusive but permits greater numerical oscillations [10]. In practice, the modified β-scheme limiter is utilized, which falls in between the minmod and Superbee limiters and can give better results

$$\mathrm{Lim}(a, b) = b \max\left\{0, \min\left[2, \min\left(\frac{1}{3}\frac{a}{b} + \frac{2}{3}, 2\frac{a}{b}\right)\right]\right\} \tag{30}$$

DOI: 10.1002/fld

3.5. Viscous fluxes discretization

Since the viscous part of the shallow water equations is parabolic, no oscillations can arise in the diffusion dominated region. So the discretization is carried out with a classical Galerkin FE P1 method which results in a centred-type scheme. For 1-D case, it is the same as the centred difference discretization in code implementation. Since the approximation of the physical variables is taken in $\mathscr{V}_h$, the components of the stress tensor and those of $\nabla\phi_i^{\triangle}$ are constant in each triangle. Any function f and its gradient are interpolated over a finite element T by

$$f(x,y)|_T = \sum_{j\in T} f(j)\phi_j|_T(x,y), \quad \text{grad}\, f(x,y)|_T = \sum_{j\in T} f(j)\text{grad}\,\phi_j|_T(x,y) = \text{constant} \tag{31}$$

Consequently, the viscous fluxes are evaluated as

$$\sum_{\triangle, P_i\in\triangle}\int_{\triangle}\mathbf{R}\cdot\nabla\phi_i^{\triangle}\,\mathrm{d}\Omega = \sum_{\triangle, P_i\in\triangle}\text{area}(\triangle)\left(R_{\triangle}^x\frac{\partial\phi_i^{\triangle}}{\partial x}+R_{\triangle}^y\frac{\partial\phi_i^{\triangle}}{\partial y}\right) \tag{32}$$

where $R_{\triangle}^x$ and $R_{\triangle}^y$ are constant values in the triangle $\triangle$.

3.6. Conservative $\mathscr{C}$-property and source terms

3.6.1. Conservative $\mathscr{C}$-property. It is well known that for a stationary shallow water problem,

$$h + z_b(x) = H = \text{const} \quad \text{and} \quad \mathbf{V} = 0 \tag{33}$$

where $\mathbf{V}$ is the velocity. A numerical scheme is said to satisfy the exact $\mathscr{C}$-property [14, 16] if the scheme can replicate the exact solution to the stationary flow problem (33).

For SWE with non-zero depth-splitting bed slope source terms, a general scheme with centred approximation of the source terms does not satisfy the exact $\mathscr{C}$-property and may give misleading results as the source terms become significant. Bermúdez and Vázquez's Q-scheme [16], and Hubbard's approach with source term decomposed [18] all satisfy the exact $\mathscr{C}$-property and can produce very accurate numerical results. Also, Zhou's SGM [20] with a water surface elevation reconstruction satisfies the exact $\mathscr{C}$-property, and the numerical scheme only uses a simple centred discretization for the source terms.

For SWE with elevation-splitting bed slope source terms, a general case of stationary problem can be written as

$$\zeta + h_b(x) + z_b(x) = H = \text{const}, \quad \zeta = \text{const}, \quad \mathbf{V} = 0 \tag{34}$$

We use a consistent discretization of bed slope source terms

$$\begin{aligned}\int_{C_i}\mathbf{S}_b\,\mathrm{d}\Omega &= \int_{C_i} g\zeta\left(0,\frac{\partial h_b}{\partial x},\frac{\partial h_b}{\partial y}\right)^{\mathrm{T}}\mathrm{d}\Omega = g\zeta_i\int_{C_i}\left(0,\frac{\partial h_b}{\partial x},\frac{\partial h_b}{\partial y}\right)^{\mathrm{T}}\mathrm{d}\Omega\\ &= g\zeta_i\sum_{j\in N(i)}\int_{\partial C_{ij}}\begin{pmatrix}0\\ h_b n_x\\ h_b n_y\end{pmatrix}\mathrm{d}\sigma\end{aligned} \tag{35}$$

DOI: 10.1002/fld

which in fact is a centred discretization for the source terms and satisfy the exact $\mathscr{C}$-property. Because of the stationary assumption (34), the interfacial reconstruction becomes $\zeta^{\mathrm{R}}=\zeta^{\mathrm{L}}$, $h^{\mathrm{R}}=\zeta^{\mathrm{R}}+h_b=h^{\mathrm{L}}$, and $\mathbf{U}^{\mathrm{R}}=\mathbf{U}^{\mathrm{L}}$, $\mathbf{F}^{\mathrm{R}}=\mathbf{F}^{\mathrm{L}}$, then the numerical flux at the left

$$\sum_{j\in N(i)}\int_{\partial C_{ij}}\mathbf{F}\cdot\mathbf{n}_{ij}\,\mathrm{d}\sigma\bigg|_{\zeta=\text{const}}=\sum_{j\in N(i)}\int_{\partial C_{ij}}\begin{pmatrix}0\\ g((\zeta+h_b)^2-h_b^2)n_x/2\\ g((\zeta+h_b)^2-h_b^2)n_y/2\end{pmatrix}\mathrm{d}\sigma$$

$$=g\zeta_i\sum_{j\in N(i)}\int_{\partial C_{ij}}\begin{pmatrix}0\\ h_bn_x\\ h_bn_y\end{pmatrix}\mathrm{d}\sigma$$

is balanced with the bed slope source terms. This proves that the numerical scheme satisfies the exact $\mathscr{C}$-property, hence $\zeta=\text{const}$ and $\mathbf{V}=0$ are preserved. 1-D proof of conservative property is one special case of two dimension which is neglected here.

3.6.2. Other source terms discretization. Besides the bed slope source terms should be balanced with the gradient flux, the other source terms integration related directly with the velocity is achieved by the classical FE manipulations:

$$\sum_{\triangle,P_i\in\triangle}\int_{\triangle}\mathbf{S}_p\phi_i^{\triangle}\,\mathrm{d}\Omega=\sum_{\triangle,P_i\in\triangle}\int_{\triangle}\sum_{k\in\triangle}(\mathbf{S}_p)_k\phi_k\phi_i\,\mathrm{d}\Omega=\sum_{\triangle,P_i\in\triangle}\sum_{k\in\triangle}(\mathbf{S}_p)_k\int_{\triangle}\phi_k\phi_i\,\mathrm{d}\Omega$$

$$=\sum_{\triangle,P_i\in\triangle}\text{area}(\triangle)\left((\mathbf{S}_p)_i+\sum_{k\in\triangle}(\mathbf{S}_p)_k\right)\frac{1}{12}\tag{36}$$

which gives second-order accuracy.

4. BOUNDARY CONDITIONS

4.1. Inflow, outflow and wall boundaries

The idea of using a Riemann solver to calculate the flux at the interface of a control volume can be used in the description of inflow, outflow, and wall boundary conditions. The sufficient conditions imposed at the boundaries combined with equations obtained from characteristics theory give the information needed for the calculation of boundary flux.

Assuming that we can neglect the source terms and that the flux has a frontal behaviour, the following Riemann invariants relationships can be obtained:

$$\frac{\mathrm{d}}{\mathrm{d}t}R^+=\frac{\mathrm{d}}{\mathrm{d}t}(u+2c)=0\quad\text{on}\ \frac{\mathrm{d}x}{\mathrm{d}t}=u+c\tag{37a}$$

$$\frac{\mathrm{d}}{\mathrm{d}t}R^-=\frac{\mathrm{d}}{\mathrm{d}t}(u-2c)=0\quad\text{on}\ \frac{\mathrm{d}x}{\mathrm{d}t}=u-c\tag{37b}$$

DOI: 10.1002/fld

so $u \pm 2c$ is constant along $u \pm c$, respectively; R^- represents the state to the left, R^+ that to the right. At a boundary the right side is outside the domain. Hence, the interface variables at the boundary can be obtained using the R^- relationship:

$$u_{\mathrm{L}}^n + 2c_{\mathrm{L}} = u_*^n + 2c_* \tag{38}$$

in which the subscripts L and $*$ indicate the left (inside) and interface variables. In general, the normal flux may then be calculated using the boundary interface variables, namely

$$\mathbf{F}(\mathbf{U}_*) \cdot \mathbf{n} = \begin{pmatrix} h_* u_*^n \\ h_* u_*^n u_* + g(h_*^2 - h_b^2) n_x/2 \\ h_* u_*^n v_* + g(h_*^2 - h_b^2) n_y/2 \end{pmatrix} \tag{39}$$

where $u_*^n = u_* n_x + v_* n_y$.

(1) *Supercritical inflow*: All the variables h_*, u_*, v_* must be imposed and no numerical boundary conditions are needed.
(2) *Sub-critical inflow*: The tangential velocity v_* and another variable must be imposed. When the water depth h_* is imposed,

$$u_*^n = u_{\mathrm{L}}^n + 2\sqrt{g}(\sqrt{h_{\mathrm{L}}} - \sqrt{h_*}) \tag{40}$$

When the velocity u_*^n is imposed,

$$h_* = ((u_{\mathrm{L}}^n - u_*^n)/2\sqrt{g} + \sqrt{h_{\mathrm{L}}})^2 \tag{41}$$

When the discharge $q = h_* u_*^n$ is imposed, c_* can be obtained by solving iteratively equation

$$2c_*^3 - (u_{\mathrm{L}} + 2c_{\mathrm{L}})c_*^2 + qg = 0 \tag{42}$$

(3) *Sub-critical outflow*: One variable must be imposed using the above formulations.
(4) *Supercritical outflow*: None of the variables must be imposed and

$$u_* = u_{\mathrm{L}}, \quad v_* = v_{\mathrm{L}}, \quad h_* = h_{\mathrm{L}} \tag{43}$$

(5) *Wall boundary*: $u_*^n = 0$ in (39) is imposed for slip wall and $u_*^\tau = v_* n_x - u_* n_y = 0$, $u_*^n = 0$ for no-slip wall.

4.2. Non-reflecting boundary condition

A useful downstream boundary condition is an outlet boundary which imposes no influence on the fluid in the domain. This is a non-reflecting boundary condition and the amplitude of the incidence wave does not vary with time. Corresponding to the characteristic lines of the inward and outward waves, the following equation [29] is utilized:

$$\frac{\partial}{\partial t}(u_n \pm 2c) + (u_n \pm c)\frac{\partial}{\partial n}(u_n \pm 2c) = gh(S_o - S_f) \tag{44}$$

DOI: 10.1002/fld

For the inward characteristic line $u_n - c$, according to the assumption that the wave amplitude is invariable, the derivative $\partial/\partial n = 0$. The resulting equations are

$$\begin{aligned} \frac{\partial}{\partial t}(u_n - 2c) &= 0 \\ \frac{\partial}{\partial t}(u_n + 2c) + (u_n + c)\frac{\partial}{\partial n}(u_n + 2c) &= gh(S_o - S_f) \end{aligned} \tag{45}$$

In this way, the values in the $(n+1)$th time-step are directly deduced from the values in the nth time-step and do not need the temporal interpolation.

5. TIME INTEGRATION

The time integrating scheme utilizes a two-step predictor–corrector sequence. So the whole method is a conservative second-order accurate, high-resolution, upwind scheme of the Godunov type

$$\mathbf{U}_i^{n+1/2}\mathrm{vol}_i = \mathbf{U}_i^n \mathrm{vol}_i - \frac{\Delta t}{2}(\mathbf{RHS})_i^n \tag{46a}$$

$$\mathbf{U}_i^{n+1}\mathrm{vol}_i = \mathbf{U}_i^n \mathrm{vol}_i - \Delta t\,(\mathbf{RHS})_i^{n+1/2} \tag{46b}$$

where

$$(\mathbf{RHS})_i^n = \sum_{j\in N(i)} \mathbf{F}(\mathbf{U}_{ij}^{\mathrm{L}}, \mathbf{U}_{ij}^{\mathrm{R}})^n \cdot \mathbf{n}_{ij} + \sum_{\triangle, P_i\in\triangle} \left[v\mathbf{R}^n \cdot \nabla\phi_i^{\triangle} + \left((\mathbf{S}_p^n)_i + \sum_{k\in\triangle} (\mathbf{S}_p^n)_k \right) \frac{1}{12} \right] \mathrm{area}(\triangle) \tag{47}$$

and the flux function $\mathbf{F}(\mathbf{U}_{ij}^{\mathrm{L}}, \mathbf{U}_{ij}^{\mathrm{R}})^n$ is evaluated by solving a local Riemann problem at each cell interface, and $\mathbf{U}_{ij}^{\mathrm{L}}, \mathbf{U}_{ij}^{\mathrm{R}}$ are the vectors of conservative variables at the left and right sides of the cell interface between node i and j, respectively.

The scheme proposed here is an explicit scheme which is restricted by a CFL-like time-step condition:

$$\Delta t = C_t \min\left(\frac{l_{\max}}{|\mathbf{V}| + c}, \frac{l_{\max}^2}{2v}, \frac{1}{2g|\mathbf{V}|/(c^2 h)} \right) \tag{48}$$

where C_t is the Courant number ($0 < C_t \leqslant 1$).

6. ONE-DIMENSIONAL NUMERICAL VERIFICATION

In this section, the FV/FEM for 1-D SWEs is verified by solving the state-of-the-art benchmark problems for SWE source terms treatment. The consistency and accuracy are demonstrated by comparing the numerical results with the analytical solutions and available numerical results.

DOI: 10.1002/fld

6.1. Tidal wave flow over an irregular bed

A tidal flow over an irregular bed proposed at a workshop on dambreak wave simulations [30] is presented to validate the method to solve the flow over an irregular bed topography. The same bed topography $z_b(x)$ is shown in Figure 3 and also used by Vázquez-Cendón [17] for verification of an upwind discretization of the bed slope source terms. The channel length is $L = 1500$ m. The initial and boundary conditions are

$$h(x, 0) = H(x), \quad H(0) = 16, \quad H(x) = H(0) - z_b(x) \tag{49a}$$

$$u(x, 0) = 0 \tag{49b}$$

and

$$h(0, t) = H(0) + 4 - 4 \sin\left[\pi\left(\frac{4t}{86\,400} + \frac{1}{2}\right)\right] \tag{50a}$$

$$u(L, t) = 0 \tag{50b}$$

Under these conditions, the tidal wave is relatively short and an asymptotic analytical solution is derived by Bermúdez and Vázquez [16] as

$$h(x, t) = H(x) + 4 - 4 \sin\left[\pi\left(\frac{4t}{86\,400} + \frac{1}{2}\right)\right] \tag{51a}$$

$$u(x, t) = \frac{(x - L)\pi}{5400h(x, t)} \cos\left[\pi\left(\frac{4t}{86\,400} + \frac{1}{2}\right)\right] \tag{51b}$$

To compare the numerical result with the asymptotic analytical solution, we choose the time $t = 10\,800$ s and $\Delta x = 15$ m based on 100 cells, which correspond to the half-risen tidal flow with maximum positive velocity. Figures 3 and 4 show the comparison of surface and velocity between the predicted numerical result and analytical solution. Excellent agreement confirms that

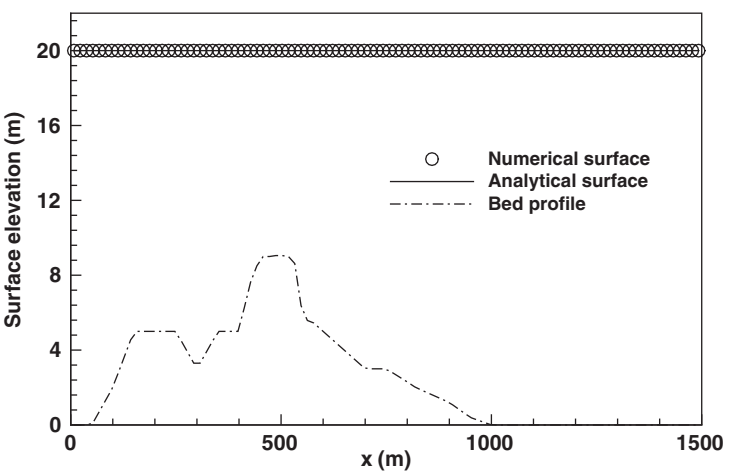

Figure 3. Tidal wave flow over an irregular bed: comparison of water surface (100 cells).

DOI: 10.1002/fld

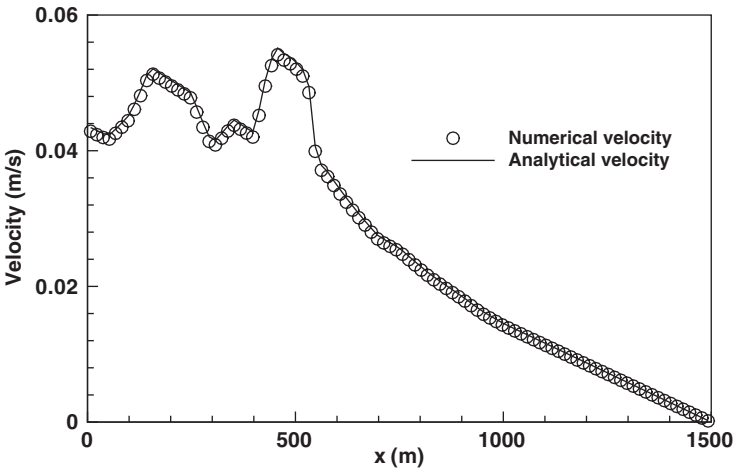

Figure 4. Tidal wave flow over an irregular bed: comparison of velocity (100 cells).

the proposed method is accurate for the numerical simulation of SWEs with a simple centred-type discretization of bed slope terms. In fact, the result validates that the consistent numerical scheme using surface elevation splitting balances the flux gradients and source terms.

6.2. *Steady flow over a 1-D hump*

A 1-D steady flow along a 25 m long 1-D channel with a hump defined by

$$z_b(x) = \begin{cases} 0.2 - 0.05(x-10)^2 & \text{if } 8\text{ m} < x < 12\text{ m} \\ 0 & \text{otherwise} \end{cases} \tag{52}$$

is a classical benchmark problem with analytical solution [30], which was also used by Vázquez-Cendón [17] and Zhou *et al.* [20] to test their schemes for the bed slope source terms. The boundary conditions determine the flow states which can be sub-critical, transcritical with or without a shock, or supercritical. The boundary conditions here are chosen to induce transcritical flow with a shock in order to verify effectiveness of the numerical scheme to predict discontinuous solution over a non-uniform bathymetry. Thus, the discharge per unit depth of $q = 0.18\ \text{m}^2/\text{s}$ is specified at the upstream boundary and the depth of $h = 0.33$ m is imposed at the downstream boundary. The numerical domain is uniformly discretized in space using 200 cells. The bed is frictionless and there is no eddy viscosity.

Figures 5 and 6 show the converged steady-state numerical predictions of the water depth and discharge along the channel. The numerical result agrees well with the analytical solution, except at near the location of the shock which may also be observed in the results reported elsewhere [17, 18, 20]. To assess the convergence history, Figure 7 shows the global relative error which is defined [20] as $R = \sqrt{\sum_i ((h_i^n - h_i^{n-1})/h_i^n)^2}$. These results indicates that the proposed method using surface elevation form can predict the discontinuous flows over irregular bed topography accurately, even though we used the simple centred-type discretization for source terms.

DOI: 10.1002/fld

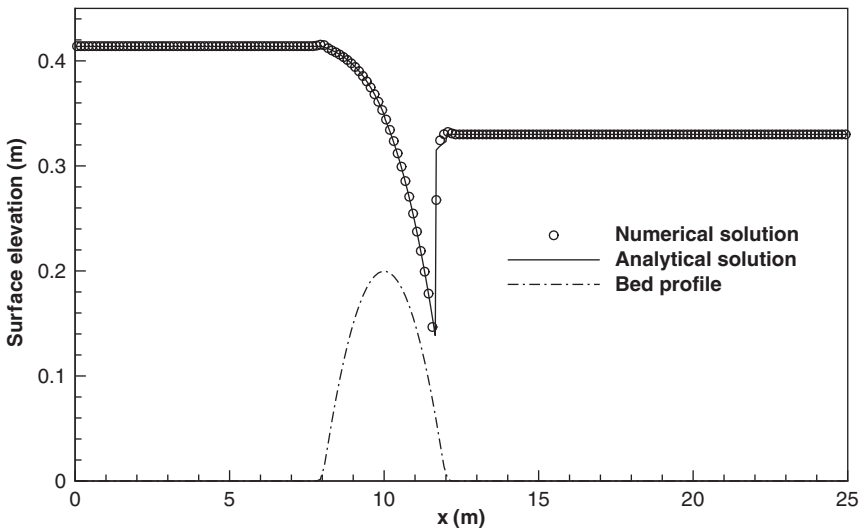

Figure 5. Steady-transcritical flow over a hump with a shock: water surface elevation.

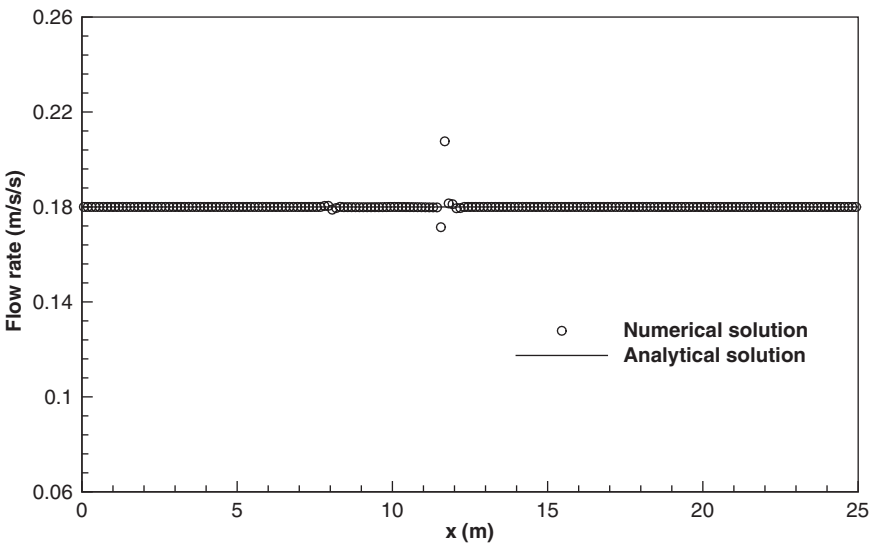

Figure 6. Steady-transcritical flow over a hump with a shock: comparison of discharge.

In order to check the accuracy properties of the numerical scheme, we apply it on the steady subcritical flow where the analytical solution is symmetric about the hump. The discharge $q = 4.42\ \mathrm{m}^2/\mathrm{s}$ is specified at the upstream boundary and the depth of $h = 2\ \mathrm{m}$ is imposed at the downstream boundary. Table I gives the convergence rate results, which indicate the numerical scheme is nearly second order of accuracy.

DOI: 10.1002/fld

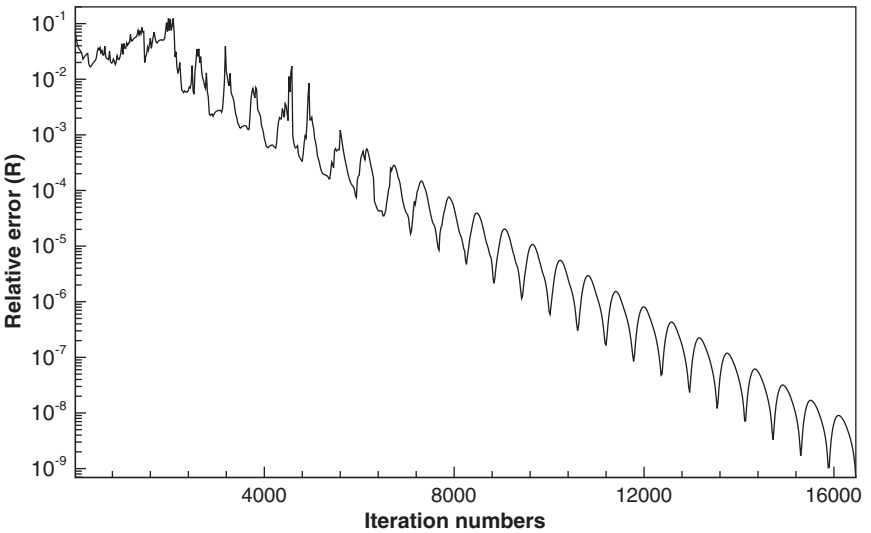

Figure 7. Steady-transcritical flow over a hump with a shock: convergence history.

Table I. Accuracy of the scheme for steady flow over a hump.

N	$L_2(h)$ error	$L_2(h)$ order	$L_2(u)$ error	$L_2(u)$ order
50	2.27×10^{-4}		3.61×10^{-4}	
100	6.59×10^{-5}	1.78	9.74×10^{-4}	1.89
200	1.77×10^{-5}	1.90	2.59×10^{-5}	1.91
400	4.61×10^{-6}	1.94	6.82×10^{-6}	1.92

7. TWO-DIMENSIONAL NUMERICAL RESULTS

7.1. Dam break problem

In order to validate the scheme for the inviscid part of the SWEs and its ability to simulate discontinuous flows, the dam break test problem is examined. A square box of $200 \times 200\,\mathrm{m}^2$ with a horizontal bed is divided into two equal compartments each measuring $200 \times 100\,\mathrm{m}^2$. The initial still water depth is 10 m on one side and 5 m on the other side of the dividing wall. At time $t = 0$, the dividing wall is instantaneously opened a distance of 75 m, as depicted in Figure 8. A bore then moves downstream as water discharges from the higher to the lower level. At the same time, a depression wave moves in the opposite direction. The problem domain is triangulated into 3646 cells (1929 vertexes and $l_{\max} \approx 5$ m) and computational model is run for up to 7.2 s after the dam break. Figures 9 and 10 show the 3-D view of the water surface elevation and the contour plot of water depth, respectively. These results agree with those reported in the literature [7, 14], and nearly give the same flow structure using high-resolution limiters [31]. As the figures show, the capturing of the downstream hydraulic jump is good and limited in two or three-triangle width.

DOI: 10.1002/fld

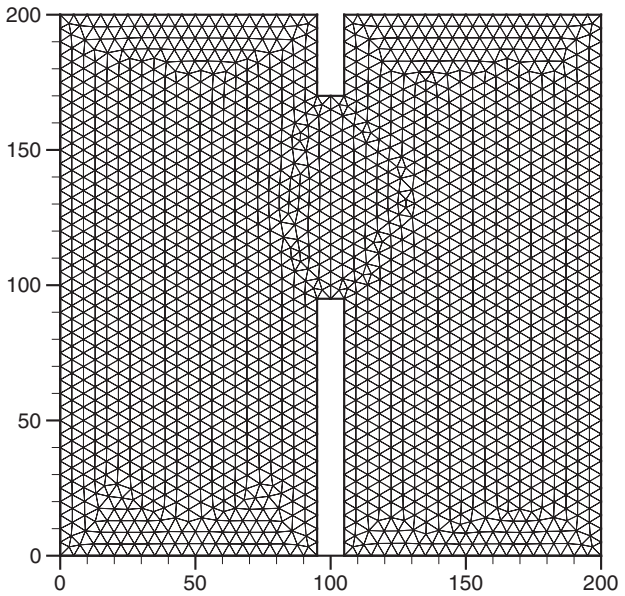

Figure 8. Definition and domain grid for dam break test.

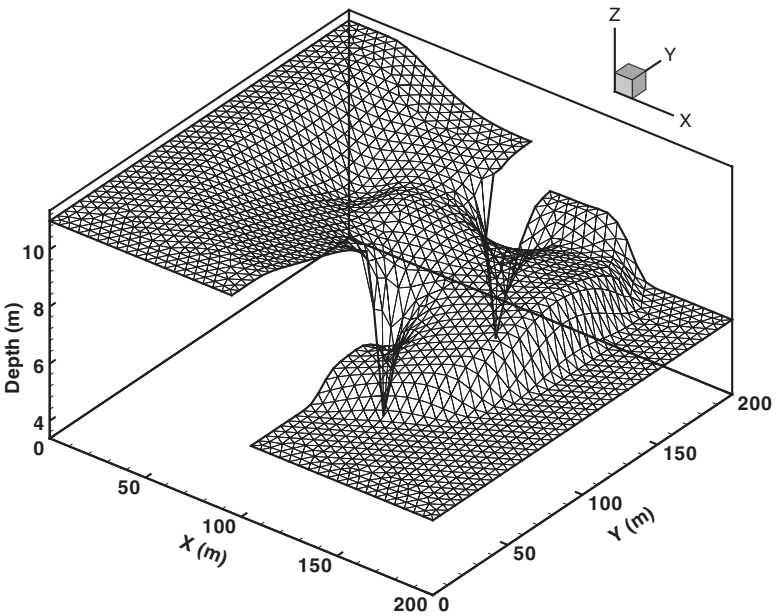

Figure 9. Water surface profile at $t = 7.2$ s after breaking of dam.

DOI: 10.1002/fld

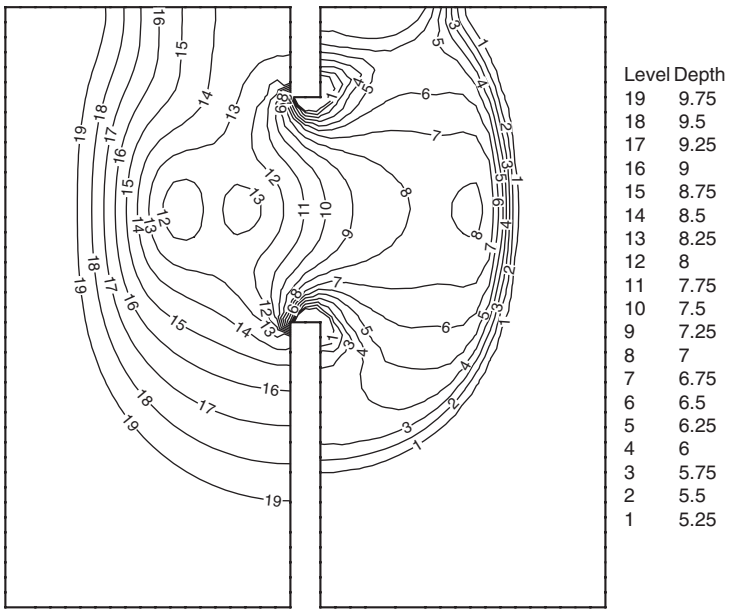

Figure 10. Contour plot of water surface elevation for dam break test.

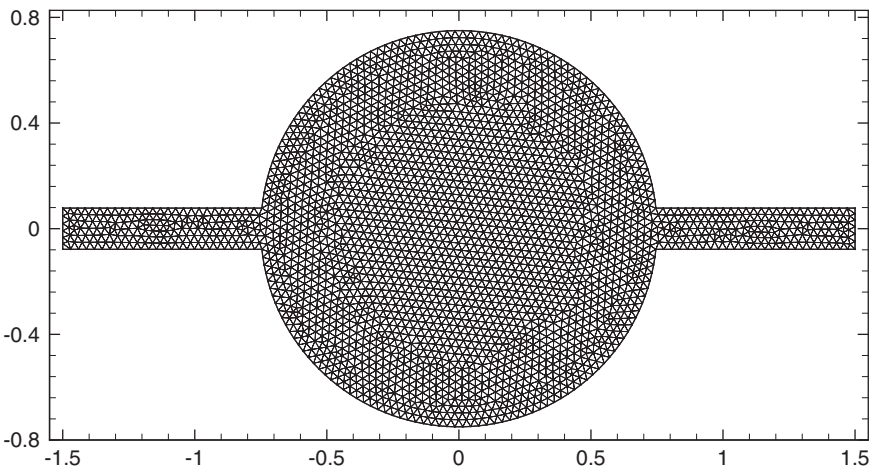

Figure 11. Definition and domain grid for jet-forced flow.

7.2. Jet-forced flow in a circular basin

A further case for testing the momentum diffusion and advective terms is examined which simulates a jet-forced flow in a circular basin. Large vorticity gradient is generated near the interior corners of the inflow and outflow stems. The circular basin (see Figure 11) has a diameter of 1.5 m,

DOI: 10.1002/fld

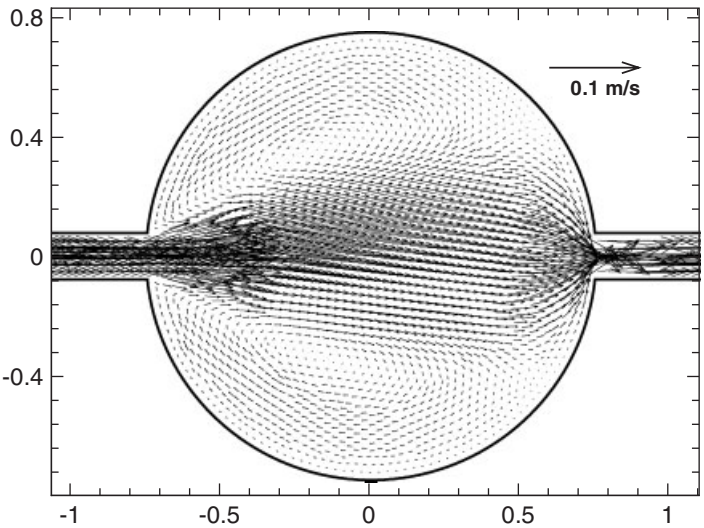

Figure 12. Velocity field at steady state for jet-forced flow.

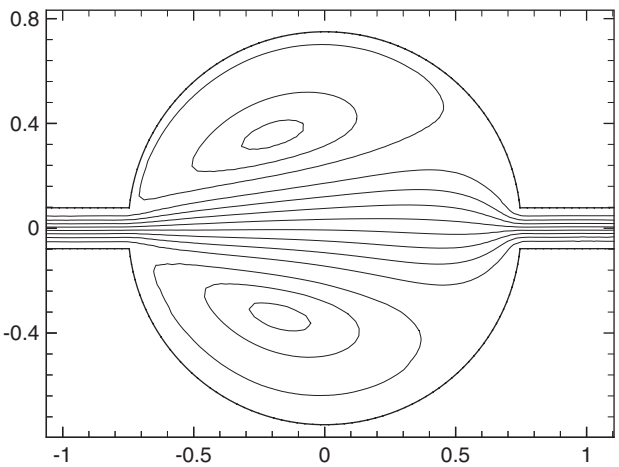

Figure 13. Streamfunction contour plot for jet-forced flow.

a uniform still water depth of 0.1 m, and symmetric inlet and outlet stems of width 0.156 m. The non-slip wall boundary condition is used, the bed stress is set to zero and the kinematic eddy viscosity is set to 0.00078 m^2/s, and the inflow velocity is 0.1 m/s, which corresponds to an inlet Reynolds number of 10.

For this test case, the computational domain is triangulated into 5356 cells. The velocity vector distribution at steady state is given in Figure 12 and the streamfunction plot is shown in Figure 13. The flow separates after entering the basin, and symmetric vortices are produced in either side of

DOI: 10.1002/fld

the fluid region, their centres displace slightly towards the inlet side of the basin. The upper vortex is anticlockwise, and the lower clockwise rotating. The overall flow pattern is in close agreement with those obtained in the literature [10, 21]. This test confirms the ability of the method to model the recirculating viscous flow within a geometrically complicated domain.

7.3. Quasi-stationary cases

A quasi-stationary test case introduced by LeVeque [19] is chosen to demonstrate the capability of the proposed method for computation involving small perturbations of the water surface. The channel has a length of 1.0 and the bed topography is defined by

$$z_b(x) = \begin{cases} 0.25[\cos(\pi(x - 0.5)/0.1) + 1] & \text{if } |x - 0.5| < 0.1 \\ 0 & \text{otherwise} \end{cases} \tag{53}$$

with $h_b(0) = 1$ and $g = 1$. The initial condition is the stationary solution $u = 0$ and

$$h(x) = \begin{cases} 1.0 - z_b(x) + \varepsilon & \text{if } 0.1 < x < 0.2 \\ 1.0 - z_b(x) & \text{otherwise} \end{cases} \tag{54}$$

Many numerical methods have difficulty with the calculations involving such small perturbations of the water surface [19]. The present solution (400 cells, $C_t = 0.2$) at time $t = 0.7$ for $\varepsilon = 0.01$ is shown in Figure 14, including a comparison with that of LeVeque [19] (1000 cells). It is shown that the new method can provide a solution of accuracy comparable to that obtained by a high-resolution Godunov-type method based on balancing the source terms and flux gradients.

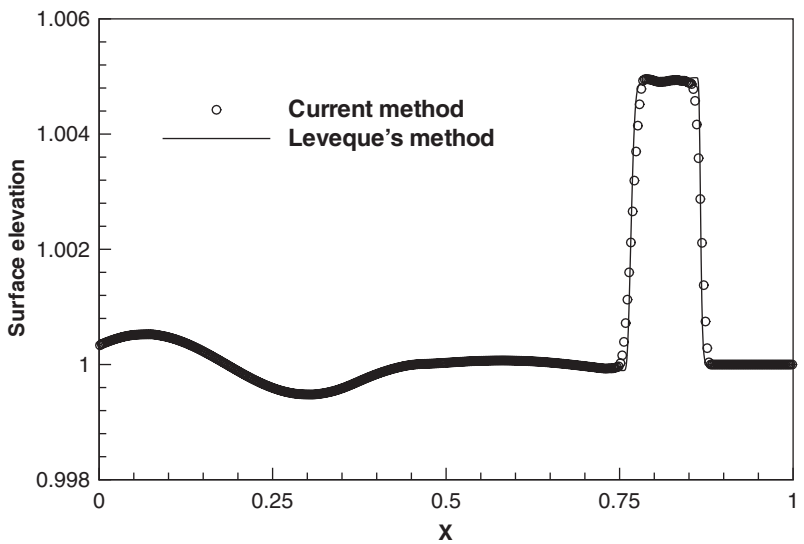

Figure 14. Quasi-stationary case: comparison of water surface elevations for $\varepsilon = 0.01$.

DOI: 10.1002/fld

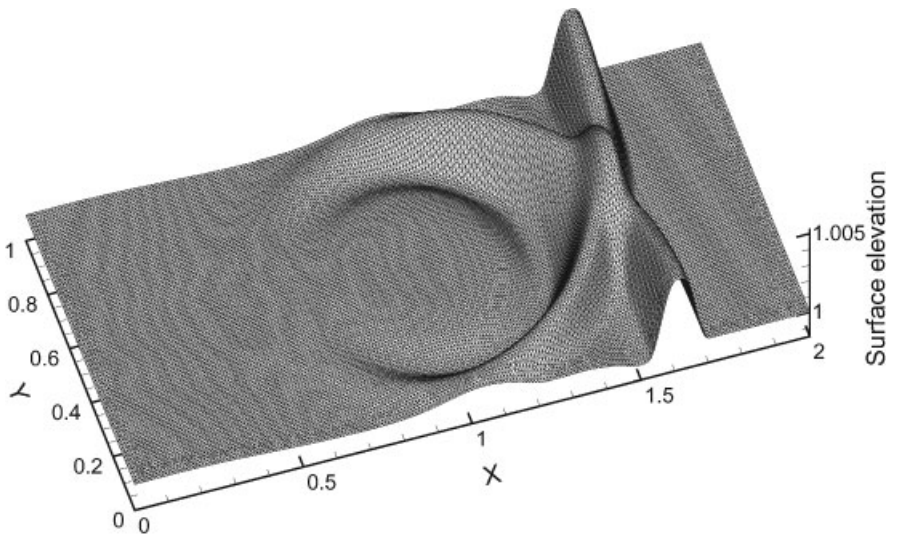

Figure 15. 2-D wave propagation past a circle hump: 3-D view of water surface.

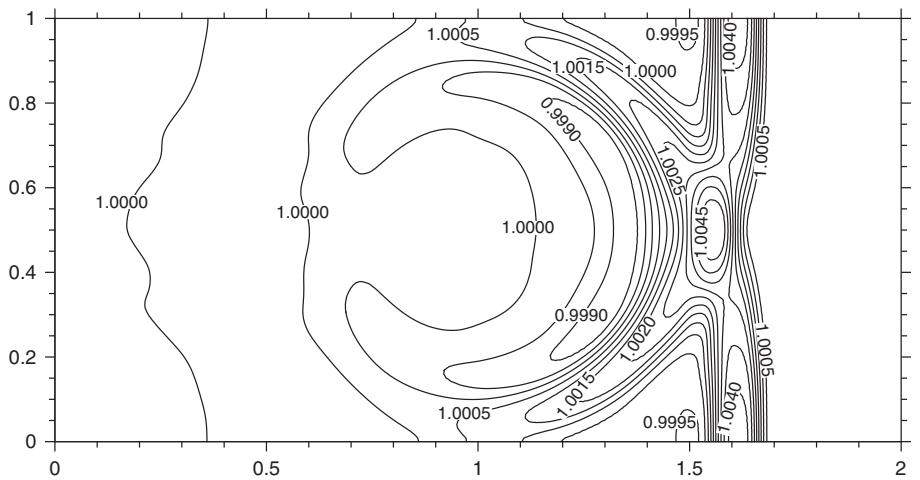

Figure 16. 2-D wave propagation past a circle hump: water surface contours.

Further test case is included in comparison with 2-D results obtained by Leveque [19]. The computation domain is $[0, 2] \times [0, 1]$ with a 2-D hump in the middle

$$z_b(x, y) = 0.8 \exp(-50((x - 0.9)^2 + (y - 0.5)^2)) \tag{55}$$

The disturbance splits into two waves, propagating left to leave the domain and right over the hump with the characteristic speeds $\pm\sqrt{gh}$. In order to resolve the waves, the non-reflecting boundary conditions are applied at $x = 0$ and 2. Figure 15 shows the 3-D surface plot obtained

DOI: 10.1002/fld

on an almost uniform 23 487 nodes, 46 372 cell triangular grids ($C_t = 0.4$) at time $t = 1.5$, and Figure 16 displays the corresponding contour plot. The plots indicate that the present solution is not polluted by unphysical numerical perturbations and agrees closely with the results obtained by LeVeque [19] and Hubbard and Garcia-Navarro [18]. These test cases show that the present method is able to handle small surface perturbation problems with the smoothly varying bathymetry.

8. CONCLUSIONS

A vertex-centred FV/FEM has been developed for solving 2-D SWEs with source terms written in a surface elevation splitting form, which balances the flux gradients and source terms naturally. The method is as simple and efficient as the conventional Godunov-type scheme for inviscid flows, and enables the source terms to be discretized with a centred-type like discretization scheme which satisfies the exact conservation property. The proposed procedure fully retains the conservative property of the parent FV method. The method has been successfully applied to a selection of steady and unsteady problems. The results indicate that the new method is accurate, simple, and robust. Further research will focus on the practical applications with complex topography.

REFERENCES

1. Abbot MB, Damsgaard A, Rodenhuis GS. SYSTEM 21, Jupiter (a design system for two-dimensional nearly horizontal flows). *Journal of Hydraulic Research* 1973; **11**:1–28.
2. Hauser J, Paap HG, Eppel D, Mueller A. Solution of the shallow water equations for complex flow domains via boundary-fitted coordinates. *International Journal for Numerical Methods in Fluids* 1985; **5**:727–744.
3. Borthwick AGL, Barber RW. River and reservoir flow modelling using the transformed shallow water equations. *International Journal for Numerical Methods in Fluids* 1992; **14**(12):1193–1217.
4. Peraire J, Zienkiweicz OC, Morgan K. Shallow water problems: a general explicit formulation. *International Journal for Numerical Methods in Engineering* 1986; **22**:547–574.
5. Westerink JJ, Luettich RA, Baptista A, Scheffner NW, Farrar P. Tide and storm-surge predictions using finite element model. *Journal of Hydraulic Engineering* 1992; **118**(10):1373–1390.
6. Glaister P. Approximate Riemann solutions for shallow water equations. *Journal of Hydraulic Research* 1988; **26**:293–305.
7. Alcrudo F, Garcia-Navarro P. A high-resolution Godunov-type scheme in finite volumes for the 2D shallow-water equations. *International Journal for Numerical Methods in Fluids* 1993; **16**(6):489–505.
8. Zhao DH, Shen HW, Tabios GQ, Lai JS, Tan WY. Finite volume two-dimensional unsteady flow model for river basins. *Journal of Hydraulic Engineering* (ASCE) 1994; **120**(7):863–883.
9. Mingham CG, Causon DM. A high resolution finite volume method for shallow water flows. *Journal of Hydraulic Engineering* (ASCE) 1998; **124**(6):605–614.
10. Anastasiou K, Chan CT. Solution of the 2D shallow water equations using the finite volume method on unstructured triangular meshes. *International Journal for Numerical Methods in Fluids* 1997; **24**(11):1225–1245.
11. Sleigh PA, Gaskell PH, Berzins M, Wright NG. An unstructured finite-volume algorithm for predicting flow in rivers and estuaries. *Computers and Fluids* 1998; **27**(4):479–508.
12. Chippada S, Dawson CN, Martinez ML, Wheeler MF. A Godunov-type finite volume method for the system of shallow water equations. *Computer Methods in Applied Mechanics and Engineering* 1998; **151**(1–2):105–129.
13. Wang ZW, Liu RX. The composite finite volume method on unstructured meshes for the two-dimensional shallow water equations. *International Journal for Numerical Methods in Fluids* 2001; **37**(8):933–949.
14. Bermúdez A, Dervieux A, Desideri JA, Vázquez ME. Upwind schemes for the two-dimensional shallow water equations with variable depth using unstructured meshes. *Computer Methods in Applied Mechanics and Engineering* 1998; **155**:49–72.
15. Ambrosi D. Approximation of shallow water equations by Roe's Riemann solver. *International Journal for Numerical Methods in Fluids* 1995; **20**:157–168.

DOI: 10.1002/fld

16. Bermúdez A, Vázquez E. Upwind methods for hyperbolic conservation-laws with source terms. *Computers and Fluids* 1994; **23**(8):1049–1071.
17. Vázquez-Cendón ME. Improved treatment of source terms in upwind schemes for the shallow water equations in channels with irregular geometry. *Journal of Computational Physics* 1999; **148**(2):497–526.
18. Hubbard ME, Garcia-Navarro P. Flux difference splitting and the balancing of source terms and flux gradients. *Journal of Computational Physics* 2000; **165**(1):89–125.
19. LeVeque RJ. Balancing source terms and flux gradients in high-resolution Godunov methods: the quasi-steady wave-propagation algorithm. *Journal of Computational Physics* 1998; **146**(1):346–365.
20. Zhou JG, Causon DM, Mingham CG, Ingram DM. The surface gradient method for the treatment of source terms in the shallow-water equations. *Journal of Computational Physics* 2001; **168**(1):1–25.
21. Rogers B, Fujihara M, Borthwick AGL. Adaptive Q-tree Godunov-type scheme for shallow water equations. *International Journal for Numerical Methods in Fluids* 2001; **35**(3):247–280.
22. Farhat C, Fezoui L, Lanteri S. Two-dimensional viscous flow computations on the connection machine: unstructured meshes, upwind schemes and massively parallel computations. *Computer Methods in Applied Mechanics and Engineering* 1993; **102**:61–88.
23. Hallo L, Ribault C, Buffat M. An implicit mixed finite-volume–finite-element method for solving 3D turbulent compressible flows. *International Journal for Numerical Methods in Fluids* 1997; **25**:1241–1261.
24. Feistauer M, Felcman J, Lukacova M, Warnecke G. Error estimates for a combined finite volume-finite element method for nonlinear convection–diffusion problems. *SIAM Journal on Numerical Analysis* 1999; **36**:1528–1548.
25. Tidriri MD. Error estimates for the hybrid finite element/finite volume methods for linear hyperbolic and convection-dominated problems. *Journal of Computational and Applied Mathematics* 2003; **156**:77–92.
26. Falconer FA. An introduction to nearly-horizontal flows. In *Coastal*, *Estuarial and Harbour Engineers Reference Book*, Abbott MB, Price WA (eds). Chapman & Hall: New York, 1993; 27–36.
27. Ma DJ. Study of high resolution numerical methods for compressible/incompressible interfacial flows. *Ph.D. Thesis*, University of Science and Technology of China, 2002.
28. Debiez C, Dervieux A. Mixed-element-volume MUSCL methods with weak viscosity for steady and unsteady flow calculations. *Computers and Fluids* 2000; **29**:89–118.
29. Su MD, Xu X, Zhu JL, Hon YC. Numerical simulation of tidal bore in Hangzhou Gulf and Qiantangjiang. *International Journal for Numerical Methods in Fluids* 2001; **36**(2):205–247.
30. Goutal N, Marel F. *Proceedings of the 2nd Workshop on Dam-break Wave Simulation*, Département Laboratoire National d'Hydraulique, Groupe Hydraulique Fluviale Electricité de France, France, HE-43/497/016/B, 1997.
31. Hubbard ME. Multidimensional slope limiters for MUSCL-type finite volume schemes on unstructured grids. *Journal of Computational Physics* 1999; **155**(1):54–74.

DOI: 10.1002/fld